

Exact Routing for Micro-Electro-Dot-Array Digital Microfluidic Biochips

Oliver Keszocze^{1,2} Zipeng Li⁴ Andreas Grimmer³ Robert Wille^{2,3}
Krishnendu Chakrabarty⁴ Rolf Drechsler^{1,2}

¹Institute of Computer Science, University of Bremen, Bremen, Germany

²Cyber-Physical Systems, DFKI GmbH, Bremen, Germany

³Institute for Integrated Circuits, Johannes Kepler University Linz, Austria

⁴Department of Electrical and Computer Engineering, Duke University, Durham, NC
{keszocze,drechsle}@informatik.uni-bremen.de {zipeng.li,krish}@duke.edu
{andreas.grimmer,robert.wille}@jku.at

Abstract—Digital microfluidics is an emerging technology that provide fluidic-handling capabilities on a chip. One of the most important issues to be considered when conducting experiments on the corresponding biochips is the routing of droplets. A recent variant of biochips uses a *micro-electrode-dot-array* (MEDA) which yields a finer controllability of the droplets. Although this new technology allows for more advanced routing possibilities, it also poses new challenges to corresponding CAD methods. In contrast to conventional microfluidic biochips, droplets on MEDA biochips may move diagonally on the grid and are not bound to have the same shape during the entire experiment. In this work, we present an exact routing method that copes with these challenges while, at the same time, guarantees to find the minimal solution with respect to completion time. For the first time, this allows for evaluating the benefits of MEDA biochips compared to their conventional counterparts as well as a quality assessment of previously proposed routing methods in this domain.

I. INTRODUCTION

Digital microfluidics is an emerging technology that provide fluidic-handling capabilities on a chip. *Digital microfluidic biochips* (DMFBs) manipulate liquids as discrete droplets of nanoliter to picoliter volumes based on the principle of *electrowetting-on-dielectric* (EWOD) [1], [2]. By reducing the rate of sample and reagent consumption, DMFBs have widely been used for various biochemical applications, such as point-of-care clinical diagnostics, large-scale immunoassays, high-throughput DNA sequencing, and protein crystallization for drug discovery [3]. However, today's DMFBs suffer from several limitations, namely (i) the constraint on the fine-grained control of droplet sizes and volumes; (ii) the lack of integrated sensors for real-time detection and (iii) the reliability/yield concern of fabricated DMFBs.

In order to overcome these limitations, a new technology, referred to as *micro-electrode-dot-array* (MEDA), has been proposed [4]–[7]. Unlike conventional DMFBs, the MEDA architecture is based on the concept of a sea-of-micro-electrodes with an array of identical basic microfluidic unit components called *microelectrode cells* [4]. Such a cell consists of a microelectrode, a control circuit, and a sensing circuit [7]. An illustration of the MEDA architecture and the microelectrode cell is presented in Fig. 1. As shown in the figure, control/sensing circuits of a microelectrode cell consist of a MUX, a D flip-flop (DFF), and an actuation/sensing module. The microelectrode cell provides fine-grained control of droplet-manipulation operations and real-time sensing/actuation for

each microelectrode in an independent manner. Moreover, in MEDA biochips, microelectrodes can dynamically be grouped together to form functional electrodes or fluidic units (e.g., mixers and diluters), which provides better reconfigurability and programmability compared to conventional DMFBs. Prototypes of MEDA biochips have been fabricated using TMS 0.35 μm technology. In these devices, a power-supply voltage of 3.3 V is used for the controlling/sensing circuits [6], [7].

With the increase in the density and area of DMFBs, it is expected that the design of such biochips (including MEDA) needs *computer-aided design* (CAD) support as strongly as conventional VLSI design does. In the past decade, noticeable research has been conducted in this regard – including solutions for allocation, resource binding, operation scheduling, module placement, and droplet routing [8], [9]. Among these stages, droplet routing represents a particularly critical challenge. Droplet routing determines the routing paths from the initial positions to the desired positions, such that unintentional droplet mixing is avoided and on-going fluidic operations are bypassed. The routing time serves as the optimization objective. There has been considerable amount of work on the droplet routing for conventional DMFBs [10]–[14].

However, due to the inherent differences between conventional DMFBs and MEDA biochips, existing droplet routing techniques cannot be utilized for MEDA biochips. Some of these differences include:

- Unlike conventional DMFBs, MEDA biochips allow for a precise and flexible control of the droplet size and droplet shape. More precisely, a droplet can dynamically change its *droplet aspect ratio* during routing by grouping together multiple microelectrodes so that functional electrodes are formed.
- When manipulating droplets with different droplet aspect ratios, the corresponding actuation and resistive forces may differ. These differences result in variable droplet velocities, which also have to be considered during droplet routing.
- Finally, MEDA biochips allow to diagonally route droplets. These diagonal movements provide a greater degree of freedom compared to conventional DMFBs where droplets can only be moved horizontally or vertically. This may be exploited for shorter routings.

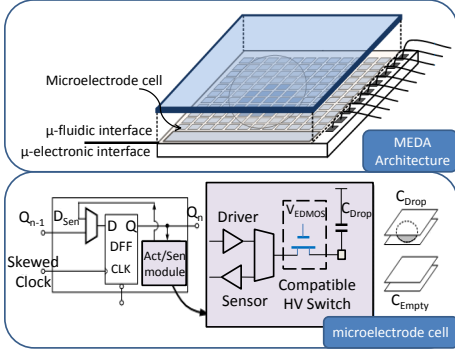


Fig. 1. Illustration of the MEDA architecture and the microelectrode cell [15].

In this work, we present the first *exact* droplet routing technique capable of handling these MEDA-specific characteristics and, at the same time, guaranteeing optimal routing results with respect to droplet routing time. To this end, all possible routings are considered. But instead of explicitly enumerating and validating all possible routings, we transform the considered routing problem into a sequence of decision problems. Each decision problem is then symbolically formulated as a *SAT Module Theories* (SMT) instance which, afterwards, is passed to a corresponding solving engine. From the obtained result, either an exact routing can be obtained or it is proven that no valid routing exists under the given constraints.

The resulting methodology allows for the first time to evaluate how MEDA-specific characteristics affect the routing time and answer the question whether MEDA biochips indeed yield advantages for routing compared to conventional DMFBs. Moreover, the proposed exact droplet routing methodology can be utilized to evaluate existing routing methods, such as [15], [16].

II. MEDA MODEL AND CONSIDERED PROBLEM

This section introduces a model for MEDA biochips which is compatible to CAD methods and, at the same time, considers the specific (physical) characteristics of this technology. Based on that, the considered routing problem is formulated and related work is discussed.

A. MEDA Model

A MEDA biochip consists of a rectangular-organized sea-of-micro-electrodes, which can be represented as a grid of size $W \times H$, where W is the width and H is the height. Each of these electrodes has a unique (x, y) -position, where $0 \leq x < W$ and $0 \leq y < H$.

An experiment executed on a MEDA biochip usually consists of multiple droplets. Therefore, let \mathcal{D} denote the set of unique identifiers for all droplets. Then, the location and size of a droplet on the grid is represented as a pair of positions. The first position specifies the lower left corner and the second position specifies the upper right corner of a droplet. This defines both, the position as well as the droplet aspect ratio and can formally be written as $((x^\downarrow, y^\downarrow), (x^\uparrow, y^\uparrow))$. The droplet aspect ratio is written as $a : b$ and can be computed via $a = x^\uparrow - x^\downarrow + 1$, $b = y^\uparrow - y^\downarrow + 1$.

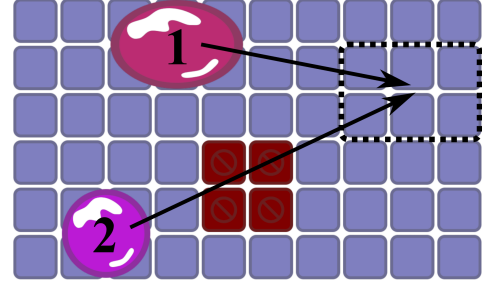


Fig. 2. MEDA routing running example: Two droplets of droplet aspect ratio of $3 : 2$ and $2 : 2$, respectively, are to be routed to the region highlighted by the dashed rectangle. The red cells are blockages and cannot be used for droplet movement.

Some electrodes of the grid may be occupied by *blockages* (e.g. on-going fluidic operations) and, therefore, cannot be used for droplet routing. The set of blockages is denoted by \mathcal{B} . Similar to droplets, the locations and sizes of these blockages can also be defined by pairs of positions.

Example 1. To denote that a droplet with a droplet aspect ratio of $3 : 2$ is located three electrodes from the left side and on the top of a 10×6 grid, we write $p = ((2, 4), (4, 5))$ (the x -coordinate is always mentioned first). Similarly, a $2 : 2$ blockage at position $(4, 1)$ can be written as $((4, 1), (5, 2))$. Fig. 2 visualizes this droplet with the ID 1 and the blockage as red block.

The movement of droplets is achieved by activating micro-electrodes, which produce a force moving the droplets. In [15], a simplified *velocity model* describes the dynamic response induced by the forces acting on a single droplet [17], [18]. The only actuation force is EWOD, and the resistive forces include plate shear force, viscous drag force, and contact-line friction force. The velocity model of [15] considers the droplet as a single mass. Furthermore, the droplets are assumed to move with an average velocity and the velocities for droplets can be calculated using their size and shape. Therefore, we define the velocity on a per-droplet basis, i.e., each droplet $d \in \mathcal{D}$ is associated with a specific velocity.

More precisely, to represent the droplet velocity in our model, we represent the velocity as the number of time steps required by a droplet to move to a neighboring position on the grid. Therefore, we discretize the routing time in T *time steps*, where one time step represents the time that the fastest droplet needs to move to a neighboring position. Accordingly, slower droplets need multiple time steps to move to a neighboring position on the grid. Formally, each droplet $d \in \mathcal{D}$ is associated with a *movement modifier* m_d , which specifies the time steps a droplet stays on the same position before reaching a new position on the grid.

Another unique characteristic of MEDA biochips is its *morphing property* which means that the droplet aspect ratio can be changed. This offers new advantages for droplet routing by allowing a higher degree of freedom, e.g., to avoid obstacles on the chip. However, due to the fact that actuation forces cannot always overcome resistive forces [19], droplets cannot be morphed arbitrarily. To represent the allowed droplet

aspect ratios an *aspect ratio library* R_d is introduced for each droplet $d \in \mathcal{D}$.

B. Routing Problem and Related Prior Work

Based on the model introduced above, the routing problem considered in this work is defined as determining routes from given source positions of droplets to their desired target positions (ideally in the minimal number of time steps). The respective routing tasks are defined in terms of *nets*.

Definition 1 (Net). A k -droplet net N is a subset of \mathcal{D} composed of k droplets that should be routed to the same target position p_N^\dagger . Each droplet $d \in N$ has an associated start position p_d^* . To ease the notation, we will also use p_d^\dagger to directly indicate the droplet's target without referring to the net the droplet belongs to. Then, the set of all nets is denoted by \mathcal{N} .

Example 2. Consider the two droplet net

$$N = \{(1, p_1^*), (2, p_2^*)\} \longrightarrow p_N^\dagger$$

with

$$\begin{aligned} p_1^* &= ((2, 4), (4, 5)), \\ p_2^* &= ((1, 0), (2, 1)), \text{ and} \\ p_N^\dagger &= ((7, 3), (9, 4)). \end{aligned}$$

The routing problem defined by this net is depicted in Fig. 2. Note that our notation, according to Definition 1, allows to write $p_1^\dagger = p_2^\dagger = p_N^\dagger$ as a shorthand.

This routing problem of MEDA biochips and also conventional DMFBs is similar to wire routing in VLSI design. Due to the analogy between digital microfluidics and digital electronics, many VLSI routing techniques can be leveraged for the droplet routing problem [20]. However, a crucial difference between classical VLSI routing and routing for DMFBs as well as MEDA biochips is that electrical nets must not be short-circuited, while droplet routes can be overlapping as long as they satisfy certain fluidic constraints (see [12]). Accordingly, dedicated droplet routing techniques have been proposed for DMFBs (see e.g., [14], [21], [22]).

However, existing routing solutions for DMFBs are not directly applicable to MEDA biochips because the routing algorithm has to consider the MEDA specific characteristics (i.e. diagonal movements, different droplet aspect ratios, and different velocities). Therefore, there is a need for specific routing solutions for MEDA biochips. To the best of our knowledge, [15], [16] are the only previous works considering droplet routing for MEDA biochips thus far.

More precisely, in [15] a technique is proposed to approximate the droplet routing time. This however basically relies on the distance between the start and target positions and neither takes the actual routing paths nor dependencies between droplets into account. In [16], an A^* -based approach is proposed to tackle the droplet routing problem for MEDA biochips. The algorithm is able to route multiple droplets with different sizes and supports diagonal movements of droplets. However, this approach employs a heuristic for which the

difference in the amount of time steps compared to the optimal solution is not yet known.

Overall, no solution exists which is capable of determining *exact* results for the routing problem of MEDA biochips. In this work, we are aiming for proposing such a solution and, by this, enable designers for the first time to obtain optimal results to be used either directly for the design of MEDA chips or to evaluate existing approximations/heuristics.

III. PROPOSED EXACT ROUTING APPROACH

This section describes the proposed exact routing approach. The general idea is to take the MEDA model and transform it into a symbolic formulation that models all possible paths of droplets including their velocities and the morphing property for a specified amount of time steps. Then, this formulation can be passed to an SMT solver, which is used to determine a satisfying assignment representing the routing of the droplets. If such an assignment can be determined, the obtained values to the variables of the symbolic formulation represent an explicit routing of all droplets. If no such assignment exists (proven by the SMT solver), the amount of considered time steps is increased until a satisfying solution is determined. This way, the determination of an exact, i.e. minimal solution, is guaranteed. In the following, details of the proposed symbolic formulation are outlined.

A. Symbolic Formulation

As the routing problem is defined by the set of nets \mathcal{N} , we can think of the biochip in terms of droplets only: everything is determined by their positions at a given point in time. We use this to define the symbolic formulation over the following variables:

Definition 2 (Symbolic Representation of Droplets). Consider a routing problem with droplets \mathcal{D} and a maximal number of time steps T . Then, a symbolic representation of all possible solutions can be defined over natural number valued variables

$$x_d^{\downarrow,t}, y_d^{\downarrow,t}, x_d^{\uparrow,t}, y_d^{\uparrow,t}$$

which are created for every droplet $d \in \mathcal{D}$ and the amount of considered time steps $1 \leq t \leq T$.

These variables describe the position and the droplet aspect ratio of droplet d at time step t . We use the following abbreviation to make the following formulas easier to read

$$p_d^t = \left((x_d^{\downarrow,t}, y_d^{\downarrow,t}), (x_d^{\uparrow,t}, y_d^{\uparrow,t}) \right)$$

Example 3. Consider again the net from Example 2 and assume $T = 5$. Then, the following variables provide a symbolic formulation of all possible routings:

$$\begin{aligned} &x_1^{\downarrow,1}, y_1^{\downarrow,1}, x_1^{\uparrow,1}, y_1^{\uparrow,1}, x_1^{\downarrow,2}, \dots, x_1^{\downarrow,5}, y_1^{\downarrow,5}, x_1^{\uparrow,5}, y_1^{\uparrow,5} \\ &x_2^{\downarrow,1}, y_2^{\downarrow,1}, x_2^{\uparrow,1}, y_2^{\uparrow,1}, x_2^{\downarrow,2}, \dots, x_2^{\downarrow,5}, y_2^{\downarrow,5}, x_2^{\uparrow,5}, y_2^{\uparrow,5}. \end{aligned}$$

For example, setting $x_1^{\downarrow,1} = 1, y_1^{\downarrow,1} = 2, x_1^{\downarrow,2} = 1, y_1^{\downarrow,2} = 3$ represents a movement of the lower left corner of droplet 1 from (1, 2) to (1, 3) between time steps 1 and 2. By allowing arbitrary assignments to these variables all possible routings

of the droplets within the considered time steps are symbolically represented.

However, an unconstrained set of variables obviously allows for arbitrary routings – including illegal configurations (e.g., overlapping droplets). In order to avoid that, semantic meaning has to be attached to the variables introduced in Definition 2.

B. Restricting Droplets to the Grid

First of all, we ensure that the droplets stay within the boundaries of the biochip, i.e. within width W and height H . The constraint ensuring that droplets may occupy valid grid cells only is given by

$$\bigwedge_{d \in \mathcal{D}} \bigwedge_{t=1}^T x_d^{\downarrow,t} < W \wedge y_d^{\downarrow,t} < H \wedge x_d^{\uparrow,t} < W \wedge y_d^{\uparrow,t} < H.$$

The lower bound of 0 is inherently enforced by the data type of the variables.

C. Enforcing the Source and Target Positions

Source and target positions must be occupied by the droplets at the beginning and at the end of the experiment, respectively. This is reflected in the constraint

$$\bigwedge_{d \in \mathcal{D}} p_d^1 = p_d^* \wedge p_d^T = p_d^\dagger.$$

Note that in case of droplets not belonging to the same net but still having identical targets, the constraints above make it impossible to find a solution. To cope with this issue, one could reformulate the constraint above in such a way that one only enforces that droplet reached their destination at least once in the considered time frame. The corresponding relaxed constraint is given by

$$\bigwedge_{d \in \mathcal{D}} \left(p_d^1 = p_d^* \wedge \bigvee_{t=2}^T p_d^t = p_d^\dagger \right).$$

D. Modeling the Droplet Movement

Droplets must not arbitrarily occupy a cell position. In fact, a droplet's corner may be present at a position p , iff it was present in the neighborhood of this position in the previous time step, i.e.

$$\bigwedge_{d \in \mathcal{D}} \bigwedge_{t=2}^T \begin{array}{l} \left| x_d^{\downarrow,t} - x_d^{\downarrow,t-1} \right| \leq 1 \wedge \left| y_d^{\downarrow,t} - y_d^{\downarrow,t-1} \right| \leq 1 \wedge \\ \left| x_d^{\uparrow,t} - x_d^{\uparrow,t-1} \right| \leq 1 \wedge \left| y_d^{\uparrow,t} - y_d^{\uparrow,t-1} \right| \leq 1 \end{array}. \quad (1)$$

The constraint above allows for every corner of the droplet to move one cell in any direction, including diagonal movement.

E. Different Droplet Velocities

As reviewed in Section II, the velocity of the moving droplets varies depending on the droplet's volume. The fastest droplet defines the base clock time and the movement of all other droplets is relative to that droplet – eventually leading to a movement modifier m_d for each droplet. Using this, the slower movement of droplets is enforced by assuming that a droplet stays on the same location for m_d time steps before

reaching a new position. This can be formulated for a single coordinate by

$$\bigwedge_{d \in \mathcal{D}} \left| x_d^{\downarrow,t} - x_d^{\downarrow,t-m_d} \right| \leq 1 \wedge \bigwedge_{i=1}^{m_d-1} x_d^{\downarrow,t-i} = x_d^{\downarrow,t-m_d}.$$

For the sake of brevity, only one coordinate is presented. The time steps considered in this constraint vary by droplet d and are given by $t = 1 + k \cdot m_d$ with $k = 1, 2, \dots$ such that $t \leq T$.

Necessary constraints that prevent droplets to move more than one position in a single time step are not shown as they are of technical nature only. This can occur in the last time steps when T is not of the form $1 + k \cdot m_d$ for a droplet d .

Note that these constraints reduce to Eq. (1) in the case of $m_d = 1$.

Example 4. Consider a droplet d with a movement modifier $m_d = 3$. The constraint for the x -coordinate of the lower left corner for time step $t = 1 + 1 \cdot m_d = 4$ is then given by

$$\left| x_d^{\downarrow,4} - x_d^{\downarrow,1} \right| \leq 1 \wedge \left(x_d^{\downarrow,3} = x_d^{\downarrow,1} \wedge x_d^{\downarrow,2} = x_d^{\downarrow,1} \right).$$

F. Aspect Ratio Constraint

Besides velocity, also the droplet aspect ratios may change. For this, the *aspect ratio library* R_d is utilized which contains all the ratios a droplet d may assume. More precisely, R_d contains tuples $r = (r_w, r_h)$ specifying the widths and heights which are allowed for the droplet d .

Example 5. To allow a droplet d to change its ratio from $3 : 3$ to $4 : 4$, the droplet aspect ratio library $R_d = \{(3,3), (3,4), (4,4)\}$ could be used. Note that this library forces the droplet to expand vertically first.

To enforce a droplet to assume the allowed ratios only, the specified widths/heights are added to the lower left corner of the droplet to make sure that the resulting coordinate is equal to the droplet's upper right corner. The corresponding constraint is given by

$$\bigwedge_{d \in \mathcal{D}} \bigwedge_{t=1}^T \bigvee_{r \in R_d} x_d^{\downarrow,t} + r_w = x_d^{\uparrow,t} \wedge y_d^{\downarrow,t} + r_h = y_d^{\uparrow,t}.$$

If one does not want to enforce a dedicated droplet aspect ratio library but to allow arbitrary ratios for the droplets (i.e., even $1 : n$ or $1 : 1$) as done in [16], it is not sufficient to simply omit the constraints above. One has to make sure that the lower left corner actually is the lower left corner by adding the constraints

$$\bigwedge_{d \in \mathcal{D}} \bigwedge_{t=1}^T x_d^{\downarrow,t} \leq x_d^{\uparrow,t} \wedge y_d^{\downarrow,t} \leq y_d^{\uparrow,t}.$$

Note that the actual change in the droplet aspect ratio comes from the movement of at least one of the droplet's corners. The constraints above merely ensure that the resulting droplet is of valid aspect ratio.

G. Blockage Constraint

Droplets should avoid moving into obstacles (called blockages). They should further keep a distance, forming a safety region around the blockages. To ensure that no droplet moves too close to a blockage, the following constraint check that no corner of the droplet is within the rectangle defined by the blockage as well as the surrounding safety region. The corresponding constraint is given by

$$\bigwedge_{d \in \mathcal{D}} \bigwedge_{b \in \mathcal{B}} \bigwedge_{t=1}^T \left(x_b^\uparrow + dist < x_d^{\downarrow,t} \vee y_b^\uparrow + dist < y_d^{\downarrow,t} \vee x_b^\downarrow - dist > x_d^{\uparrow,t} \vee y_b^\downarrow - dist > y_d^{\uparrow,t} \right). \quad (2)$$

Here, $dist$ defines the safety margin (usually 1) and \mathcal{B} is the set of all blockages.

Example 6. Consider again the running example shown in Fig. 2. The blockage is at location $((5, 2), (6, 3))$. Fixing the safety margin to 1, the corresponding constraint for the first time step is

$$\begin{aligned} 6 + 1 < x_1^{\downarrow,1} \vee 3 + 1 < y_1^{\downarrow,1} \vee 5 - 1 > x_1^{\uparrow,1} \vee 2 - 1 > y_1^{\uparrow,1} \\ 6 + 1 < x_2^{\downarrow,1} \vee 3 + 1 < y_2^{\downarrow,1} \vee 5 - 1 > x_2^{\uparrow,1} \vee 2 - 1 > y_2^{\uparrow,1}. \end{aligned}$$

H. Fluidic Constraints

Finally, it has to be prevented that droplets are moving too close to each other and, hence, would cause unintended mixings. Therefore, droplets themselves need to be considered as blockages – leading to so-called fluidic constraint (this constraint has been introduced in [12]). This constraint do not apply to droplets belonging to the same net as they are intended to mix in the end anyway.

The corresponding constraint is almost identical to the blockage constraint in Eq. (2) and is given by

$$\bigwedge_{t=1}^T \bigwedge_{\substack{N, N' \in \mathcal{N} \\ N \neq N'}} \bigwedge_{\substack{d \in N \\ d' \in N'}} x_d^{\uparrow,t} + dist < x_{d'}^{\downarrow,t} \vee y_d^{\uparrow,t} + dist < y_{d'}^{\downarrow,t} \vee \dots$$

Note that, for sake of brevity, we omitted the terms for the upper right corner and the dynamic fluidic constraint taking into account multiple time steps.

I. Solving the Instance and Determining the Routes

Passing the formulation described above to an SMT solver either yields a satisfying assignment to all variables or a proof that no such assignment exists. In the latter case, this also proves that no solution exists, which routes the considered droplets from the start to the target positions within the considered number of time steps. In the former case, a valid routing can be obtained from all assignments. More precisely, each assignment to the variables p_d^t represents the position of droplet d at time step t . Considering this for all droplets $d \in \mathcal{D}$ and all time steps $1 \leq t \leq T$ eventually yields the desired routes.

IV. EXPERIMENTS

The proposed routing methodology allows for an *exact* evaluation of the benefits of MEDA biochips (compared to conventional biochips) as well as an *exact* comparison to previously proposed solutions. In this section, we are summarizing the correspondingly obtained findings. To this end, we took the commonly used benchmarks (see e.g., [16], [23]) and – similarly to [16] – scaled them up to reflect the high density of microelectrode cells. This allows for a fair comparison to the results reported in prior work. All experiments have been conducted on an Intel machine with 3.5 GHz and 32 GB of main memory.

A. Conventional DMFBs versus MEDA Biochips

As already discussed above, MEDA biochips allow for a more advanced droplet routing additionally employing (1) different droplet aspect ratios, (2) variable droplet velocities and (3) diagonal movements. Using the proposed methodology, we can, for the first time, evaluate the precise effects of these more advanced routing capabilities. To this end, we compare the minimal number of time steps obtained by an exact routing approach for conventional DMFBs (taken from [14]) to the minimal number of time steps obtained by the proposed approach for MEDA biochips. Moreover, to investigate the impact of droplet aspect ratios and diagonal movements, results for MEDA biochips are provided with these features disabled/enabled.

Table I shows the resulting numbers for four different benchmark sets (consisting of several routing problems) using the different settings. The maximum and average number of time steps needed to perform the respective routings on the benchmark sets are given (denoted as $\max T$ and $\text{avg. } T$, respectively)¹. For sake of completeness, we additionally provide the run-time (in CPU seconds) needed to determine the results.

These numbers clearly show the benefits of MEDA chips: Using a conventional setup, i.e. no diagonal movement and restricted droplet aspect ratios, leads to results that are almost identical to conventional biochips. But the more “freedom” is allowed (i.e. diagonal movements, arbitrary droplet aspect ratios), the better (i.e., smaller) the number of needed time steps. The capability of diagonal movements has the most significant impact, while the impact of different droplet aspect ratios is moderate. Restricting the droplet aspect ratio is a reasonable choice as the droplets’ volumes do not change during routing. This means that a model allowing to change the droplet aspect ratio from 2 : 1 to 10 : 23 or from 6 : 7 to 1 : 1 would result in droplets becoming arbitrarily thin or thick, respectively.

B. Comparison to Previous Work

Recall that, thus far, only an approximation of the actual routing time [15] or a heuristic solution for the determination of the actual routing [16] exists for MEDA biochips. In

¹We normalize our results by computing the equivalent arrival times as proposed in [16]. This enables us to compare ourselves against the results obtained from conventional DMFB routing. This is further necessary as in [16] only normalized data is published.

TABLE I
CONVENTIONAL DMFBs VERSUS MEDA BIOCHIPS.

Name	Exact routing on conventional DMFB [14]			Exact routing on MEDA biochip											
				w/o diagonal movement						w/ diagonal movement					
				w/ restricted aspect ratios			w/o restricted aspect ratios			w/ restricted aspect ratios			w/o restricted aspect ratios		
	max T	avg. T	CPU [s]	max T	avg. T	CPU [s]	max T	avg. T	CPU [s]	max T	avg. T	CPU [s]	max T	avg. T	CPU [s]
in-vitro 1	18.00	11.20	1091.80	18.00	11.67	1285.73	18.00	11.67	731.42	15.00	9.09	599.27	15.00	9.09	152.66
in-vitro 2	16.00	10.07	793.90	16.00	9.64	3140.30	16.00	9.64	877.48	11.67	7.12	170.89	11.67	7.12	87.45
protein 1	20.00	15.28	9754.20	20.00	15.28	16289.99	20.00	15.28	4667.17	17.67	14.21	2782.00	17.67	12.47	909.20
protein 2	20.00	9.53	3950.50	20.00	9.49	5918.80	18.67	9.44	1696.27	17.33	7.73	1084.11	16.67	7.54	729.28

Exact routing on MEDA biochips: w/ restricted droplet aspect ratios means that the droplet's shape is restricted to the shape library $\{(3, 3), (3, 4), (4, 3), (4, 4)\}$; otherwise (w/o restricted aspect ratios), arbitrary droplet aspect ratios can be applied. T denotes the amount of time steps necessary to perform the routing.

TABLE II
COMPARISON TO PREVIOUS WORK.

Name	Approx. of [15]		Heuristic of [16]		Prop. methodology	
	max T	avg. T	max T	avg. T	max T	avg. T
in-vitro 1	12.33	8.2	15.33	9.55	15.00	9.09
in-vitro 2	10.67	6.33	11.33	7.29	11.67	7.12
protein 1	15.67	9.36	18.67	12.30	17.67	12.47
protein 2	12.33	5.25	16.67	7.48	16.67	7.54

both cases, it is unclear how far these approximated/heuristic solutions are from the actual minimum (cf. discussion in Sec. II). Using the proposed methodology, this evaluation can be made for the first time. Corresponding numbers are provided in Table II.

They clearly show that the work of [15] is indeed overly optimistic. For all benchmarks, a smaller number of time steps is approximated than required by a minimal routing. This under-approximation is caused by the fact that only distances are used to estimate the number of time steps. Blockages or cells blocked by other droplets are not considered at all. In contrast, the work of [16] generates much better results. In fact, our methodology allowed to show that routings heuristically determined by the A*-based approach are close to the optimum. Note that we explicitly model the change in aspect ratio. This explains the shorter max T for the in-vitro 2 experiment when compared to [16].

V. CONCLUSIONS

In this work, we proposed an exact routing methodology for micro-electrode-dot-array biochips. In contrast to conventional biochips, they allow for more advanced routing capabilities such as diagonal movements and different droplet aspect ratios, but also yield droplets with different velocities. The proposed methodology considers these characteristics and, at the same time, ensures the determination of exact, i.e. minimal, routings. For the first time, this allows for an exact evaluation of the benefits of MEDA chips compared to conventional DMFBs. Besides that, we were able to check the quality of previously proposed approximations and heuristics.

ACKNOWLEDGEMENTS

The work of K. Chakrabarty was supported in part by a Humboldt Research Award from the Alexander von Humboldt Research Foundation, Germany.

REFERENCES

- [1] M. Pollack et al. Electrowetting-based actuation of liquid droplets for microfluidic applications. *Applied Physics Letters*, 77:1725–1726, 2000.
- [2] R. Fair. Digital microfluidics: is a true lab-on-a-chip possible? *Microfluidics and Nanofluidics*, 3:245–281, 2007.
- [3] K. Choi et al. Digital microfluidics. *Annual Review of Analytical Chemistry*, 5:413–440, 2012.
- [4] G. Wang et al. Digital microfluidic operations on micro-electrode dot array architecture. *IET Nanobiotechnology*, 5:152–160, 2011.
- [5] G. Wang et al. Field-programmable lab-on-a-chip based on micro-electrode dot array architecture. *IET Nanobiotechnology*, 8:163–171, 2013.
- [6] K. Lai et al. An intelligent digital microfluidic processor for biomedical detection. *Journal of Signal Processing Systems*, 78:85–93, 2015.
- [7] K. Lai et al. A field-programmable lab-on-a-chip with built-in self-test circuit and low-power sensor-fusion solution in 0.35 μm standard CMOS process. In *Asian Solid-State Circuits Conference*, pages 1–4, 2015.
- [8] K. Chakrabarty. Design automation and test solutions for digital microfluidic biochips. *IEEE Trans. on Circuits and Systems*, 57:4–17, 2010.
- [9] T.-Y. Ho et al. Digital microfluidic biochips: A vision for functional diversity and more than moore. In *Int'l Conf. on CAD*, pages 578–585, 2010.
- [10] Y. Zhao et al. Cross-contamination avoidance for droplet routing in digital microfluidic biochips. *IEEE Trans. on CAD*, 31:817–830, 2012.
- [11] Q. Wang et al. Practical functional and washing droplet routing for cross-contamination avoidance in digital microfluidic biochips. In *Design Automation Conf.*, pages 1–6. IEEE, 2014.
- [12] F. Su et al. Droplet routing in the synthesis of digital microfluidic biochips. In *Design, Automation and Test in Europe*, pages 1–6, 2006.
- [13] O. Keszocze et al. A general and exact routing methodology for digital microfluidic biochips. In *Int'l Conf. on CAD*, pages 874–881, 2015.
- [14] O. Keszocze, R. Wille, and R. Drechsler. Exact routing for digital microfluidic biochips with temporary blockages. In *Int'l Conf. on CAD*, pages 405–410, 2014.
- [15] Z. Li et al. High-level synthesis for micro-electrode-dot-array digital microfluidic biochips. In *Design Automation Conf.*, pages 146–151. ACM, 2016.
- [16] Z. Chen et al. Droplet routing in high-level synthesis of configurable digital microfluidic biochips based on microelectrode dot array architecture. *BioChip Journal*, 5(4):343–352, 2011.
- [17] V. Bahadur et al. An energy-based model for electrowetting-induced droplet actuation. *Journal of Micromechanics and Microengineering*, 16:1494–1503, 2006.
- [18] H. Oprins et al. Modeling and control of electrowetting induced droplet motion. *Micromachines*, 3:150–167, 2012.
- [19] E. Baird et al. Electrostatic force calculation for an ewod-actuated droplet. *Microfluidics and Nanofluidics*, 3:635–644, 2007.
- [20] N. Sherwani. *Algorithms for VLSI physical design automation*. Springer Science & Business Media, 2012.
- [21] M. Cho and D. Z. Pan. A high-performance droplet routing algorithm for digital microfluidic biochips. *IEEE Trans. on CAD*, 27(10):1714–1724, 2008.
- [22] T.-W. Huang and T.-Y. Ho. A fast routability- and performance-driven droplet routing algorithm for digital microfluidic biochips. In *Int'l Conf. on Comp. Design*, pages 445–450. IEEE, 2009.
- [23] O. Keszocze, R. Wille, T.-Y. Ho, and R. Drechsler. Exact One-pass Synthesis of Digital Microfluidic Biochips. In *Design Automation Conf.*, pages 1–6, 2014.